MOEM

Modern Electronic Materials 2023; 9(3): 123–131
DOI 10.3897/j.moem.9.3.115614

Research Article

Effect of heat treatment on the structure and mechanical properties of zirconia crystals partially stabilized with samarium oxide

Mikhail A. Borik[1], Aleksej V. Kulebyakin[1], Elena E. Lomonova[1], Filipp O. Milovich[1], Valentina A. Myzina[1], Polina A. Ryabochkina[2], Natalya V. Sidorova[2], Nataliya Yu. Tabachkova[1], Artem S. Chislov[1]

1 Prokhorov General Physics Institute of the Russian Academy of Sciences, 38 Vavilov Str., Moscow 119991, Russian Federation

2 National Research Ogarev Mordovia State University, 68 Bolshevistskaya Str., Saransk 430005, Republic of Mordovia, Russian Federation

Corresponding author: Nataliya Yu. Tabachkova (ntabachkova@gmail.com)

Received 18 September 2023 ♦ **Accepted** 2 October 2023 ♦ **Published** 11 October 2023

Citation: Borik MA, Kulebyakin AV, Lomonova EE, Milovich FO, Myzina VA, Ryabochkina PA, Sidorova NV, Tabachkova NYu, Chislov AS (2023) Effect of heat treatment on the structure and mechanical properties of zirconia crystals partially stabilized with samarium oxide. *Modern Electronic Materials* 9(3): 123–131. https://doi.org/10.3897/j.moem.9.3.115614

Abstract

The effect of high-temperature treatment in different media on the phase composition, microhardness and fracture toughness of $(ZrO_2)_{1-x}(Sm_2O_3)_x$ crystals with $x = 0.02 \div 0.06$ has been studied. The crystals have been grown using direction melt crystallization in a cold skull. The crystals have been heat treated at 1600 °C for 2 h in air and in vacuum. The phase composition of the crystals has been studied using X-ray diffraction and Raman scattering. We show that samarium cations enter the ZrO_2 lattice mainly in a trivalent charge state and do not change their charge after air or vacuum annealing. The as-annealed phase composition has changed in all the test crystals except for the $(ZrO_2)_{0.94}(Sm_2O_3)_{0.06}$ composition. After air or vacuum annealing the $(ZrO_2)_{1-x}(Sm_2O_3)_x$ crystals with $0.002 \le x \le 0.05$ contain a monoclinic phase. The $(ZrO_2)_{0.94}(Sm_2O_3)_{0.06}$ crystals contain two tetragonal phases (t and t') with different tetragonality degrees. After air or vacuum annealing of the $(ZrO_2)_{0.94}(Sm_2O_3)_{0.06}$ crystals the lattice parameters of the t and t' phases change in opposite manners, suggesting that the tetragonality degree of the t phase increases whereas the tetragonality degree of the t' phase decreases. The microhardness and fracture toughness of the as-annealed crystals depend on the Sm_2O_3 concentration in the solid solutions. The formation of the monoclinic phase in the $(ZrO_2)_{1-x}(Sm_2O_3)_x$ crystals with $0.037 \le x \le 0.05$ significantly reduces the microhardness and fracture toughness of the crystals. Annealing of the $(ZrO_2)_{0.94}(Sm_2O_3)_{0.06}$ crystals triggers more efficient hardening mechanisms and thus increases the fracture toughness of the crystals. We show that air or vacuum annealing of the $(ZrO_2)_{0.94}(Sm_2O_3)_{0.06}$ crystals increases the fracture toughness of the crystals by 1.5 times as compared with that of the as-grown crystals.

Keywords

zirconia, ZrO_2–Sm_2O_3, crystal growth, microhardness, fracture toughness, optical spectroscopy, Raman scattering

1. Introduction

Zirconia based materials are distinguished by good mechanical and heat insulating properties combined with high chemical inertness that provide for their wide application in high-temperature engineering [1–3]. The good mechanical properties of zirconia based tetragonal solid solutions originate, primarily, from the transformation hardening mechanism. This hardening mechanism is associated with the possibility of a transition from the tetragonal phase to the monoclinic one. The stress-induced phase transition absorbs the energy of stress thus stopping the propagation of microcracks. However, it is the tetragonal phase that limits the maximum operation temperature of zirconia based materials because high-temperature treatment can initiate undesired transformation of the tetragonal phase to the monoclinic one in the material bulk. Materials that undergo thermocycling and high-temperature impact during operation are required to meet stringent requirements to the stability of their thermophysical and mechanical properties which finally determine their durability. The development of advanced high-temperature engineering imposes new requirements to the operation temperature range of materials. Therefore, the search for new thermal-barrier materials has two main trends: first, the use of materials other than zirconia [4, 5], and second, stabilization of the tetragonal or cubic phases in zirconia using additional oxides other than yttria or combinations of several rare-earth element oxides [6–10]. Zirconia has high isomorphic capacity and allows introducing a wide range of impurities, e.g. rare-earth, alkaline-earth and transition elements [11–13]. Introduction of several oxides is used for modifying the physicochemical properties of the zirconia based solid solutions and for increasing their phase stability.

A large number of works have dealt with the dependence of the chemical, composition, structure and mechanical and thermophysical properties on the composition and synthesis and heat treatment conditions of the ZrO_2–Y_2O_3 solid solutions [14–17]. However there are also works that have dealt with the effect of annealing on the structure and properties of the ZrO_2 solid solutions stabilized with other oxides [18–20].

An increase in the cation radius of stabilizing oxides leads to an increase in the temperature of the phase transition from the high-temperature cubic phase to the two-phase region, in accordance with the ZrO_2 – stabilizing oxide phase diagram. From this viewpoint the synthesis of crystals with a predominant tetragonal phase that does not undergo a transition to the monoclinic phase can be implemented via the use of stabilizing oxides with greater ionic radii of cations than Y^{3+}. The ionic radius of trivalent samarium cations is greater than those of gadolinium and yttrium. It has been shown [21] that ZrO_2 tetragonal solid solutions stabilized with Sm_2O_3 have a greater fracture toughness than ZrO_2 solid solutions stabilized with Y_2O_3. Studies of the effect of thermal annealing on the high-temperature stability of the structure and mechanical properties of the solid solutions are of primary importance for the practical applications of the material.

The aim of this work is to study the effect of high-temperature annealing in air and in vacuum on the phase composition and mechanical properties of ZrO_2 based solid solutions partially stabilized with Sm_2O_3.

2. Experimental

$(ZrO_2)_{1-x}(Sm_2O_3)_x$ solid solution crystals with $x = 0.02 \div 0.06$ were grown using directional melt crystallization in a 100 mm diam. water-cooled crucible with direct induction heating. The power source was a 63 kW high-frequency generator at 5.28 MHz. The raw powders (main material content at least 99.99 %) were preliminarily mechanically mixed before loading into the crucible. The charge weight was 4.5–5 kg. Melting was initiated using metallic zirconium. The melt was crystallized by removing the crucible from the heated zone at a 10 mmph speed. The cross-sections and lengths of the as-grown crystals were 5 to 20 mm and 30 to 40 mm, respectively.

The crystals were heat treated at 1600 °C in air and in vacuum. The density of the specimens was measured by hydrostatic weighing. The density measurement error was 0.1 %.

The phase composition of the crystals was studied using X-ray diffraction and Raman spectroscopy on a Bruker D8 diffractometer and a Renishaw in Via microscope and spectrometer, respectively. Wafers for the studies were cut from the middle parts of the crystals. Crystals grown using directional melt crystallization in a cold skull have no preferential growth directions. Therefore test crystal orientations were verified on the X-ray diffractometer and then wafers were cut perpendicular to the <100> direction.

The microhardness and cracking resistance of the crystals were compared via indentation on the {001} plane at different specimen rotation angles in their planes. The instruments used were a DM 8 B AUTO microhardness tester with a Vickers indenter (maximum load 20 N) and a Wolpert Hardness Tester 930 with a minimum load of 50 N. After cutting the specimens were subjected to chemomechanical polishing for damaged surface layer removal. The polishing agents were compositions of nanometer-sized amorphous silica particles. The roughness of the as-polished surfaces was 0.3–0.5 nm, and the surfaces contained no microscratches and were leveled and smooth.

The cracking resistance (K_{1c}) was calculated using the formula [22]:

$$K_{1c} = 0{,}035(L/a)^{-1/2}(CE/H)^{2/5}Ha^{1/2}C^{-1}, \quad (1)$$

where K_{1c} is the stress intensity coefficient (MPa·m$^{1/2}$); L is the radial crack length (m); a is the indentation half-

width (m); C is the constraint factor (=3); E is Young's modulus (Pa); H is the microhardness (Pa).

The K_{1c} parameter was calculated for radial cracks around indentations if the crack length met the criterion ($0.25 \le l/a \le 2.5$).

3. Results and discussion

The high-temperature stability of the structure and mechanical properties of the $(ZrO_2)_{1-x}(Sm_2O_3)_x$ solid solution crystals with x = 0.02, 0.028, 0.032, 0.037, 0.04, 0.05 и 0.06 was studied in different media. Hereinafter te crystal compositions will be denoted as xSmSZ where x is the Sm_2O_3 stabilizing oxide concentration in mol.%. Figure 1 shows the appearance of the 3.7SmSZ crystals before and after heat treatment in air and in vacuum. The crystals of other compositions had similar appearance.

After air annealing the color of the crystal changed, whereas after vacuum annealing the crystals became black. The dark color of the crystals was caused by nonstoichiometric vacancies whose formation during crystal vacuum annealing leads to the formation of an absorption band in the visible region. Air and vacuum annealing of the $(ZrO_2)_{1-x}(Sm_2O_3)_x$ crystals of all the experimental compositions except 6SmSZ led to noticeable changes in their surface appearance.

Changes in the crystal surface morphology were examined under an optical microscope. Figure 2 shows the surfaces of the 3.7SmSZ and 6SmSZ before and after air and vacuum annealing.

The surface of the as-grown 3.7SmSZ crystals was smooth and uniform. Air and vacuum annealing of the 3.7SmSZ crystals led to the formation of a surface texture. The surface texture of the crystals after vacuum annealing is more pronounced and contains larger structural features. Similar surface morphology changes were observed for the 4SmSZ and 5SmSZ crystals. The surface of the $(ZrO_2)_{1-x}(Sm_2O_3)_x$ crystals with $x < 0.037$ appeared non-uniform before annealing. Annealing of those crystals increased their surface roughness and the number of microcracks. Only the as-annealed 6SmSZ crystals exhibited no surface morphology changes. The surface of the 6SmSZ crystals appeared smooth and uniform both before and after annealing.

Study of the phase composition of the $(ZrO_2)_{1-x}(Sm_2O_3)_x$ crystals showed that air and vacuum annealing led to the formation of the monoclinic phase in the 3.7SmSZ, 4SmSZ and 5SmSZ crystals and increased the content of the monoclinic phase in the 3.2SmSZ ones. Figure shows by way of example a diffraction pattern for the 3.7SmSZ crystals after air annealing.

The tetragonal structure of the 6SmSZ crystals persisted after air and vacuum annealing. However, annealing led to changes in the lattice parameters and hence changes in the tetragonality degree of the phases. The ratio of the phases did not change any appreciably. Table 1 summarized data on the phase compositions, lattice parameters and tetragonality degrees of the 6SmSZ crystals before and after heat treatment.

The data in Table 1 suggest that the phase susceptible to a tetragonal-to-monoclinic transition under external stress exhibits a decrease in the lattice parameter a and an increase in the lattice parameter c after air annealing. This reduces the tetragonality degree of the t phase. The trend of changes in the lattice parameters of the t' phase was opposite. Air annealing increased its lattice parameter a and increased its lattice parameter c. Thus, air annealing causes opposite changes in the lattice parameters of the t and t' phases.

Vacuum annealing of the crystals reduced the lattice parameters of the crystals, potentially indicating the formation of nonstoichiometric vacancies. However, the tetragonality degree of the t phase increased after vacuum annealing whereas the tetragonality degree of the t' phase decreased as compared with those of the as-grown crystals.

The observed changes in the tetragonality degree of the crystals after air and vacuum annealing suggest that the content of Sm_2O_3 in the t phase decreases, while that

Figure 1. Appearance of 3.7SmSZ crystals (*a*) before and after (*b*) air and (*c*) vacuum annealing

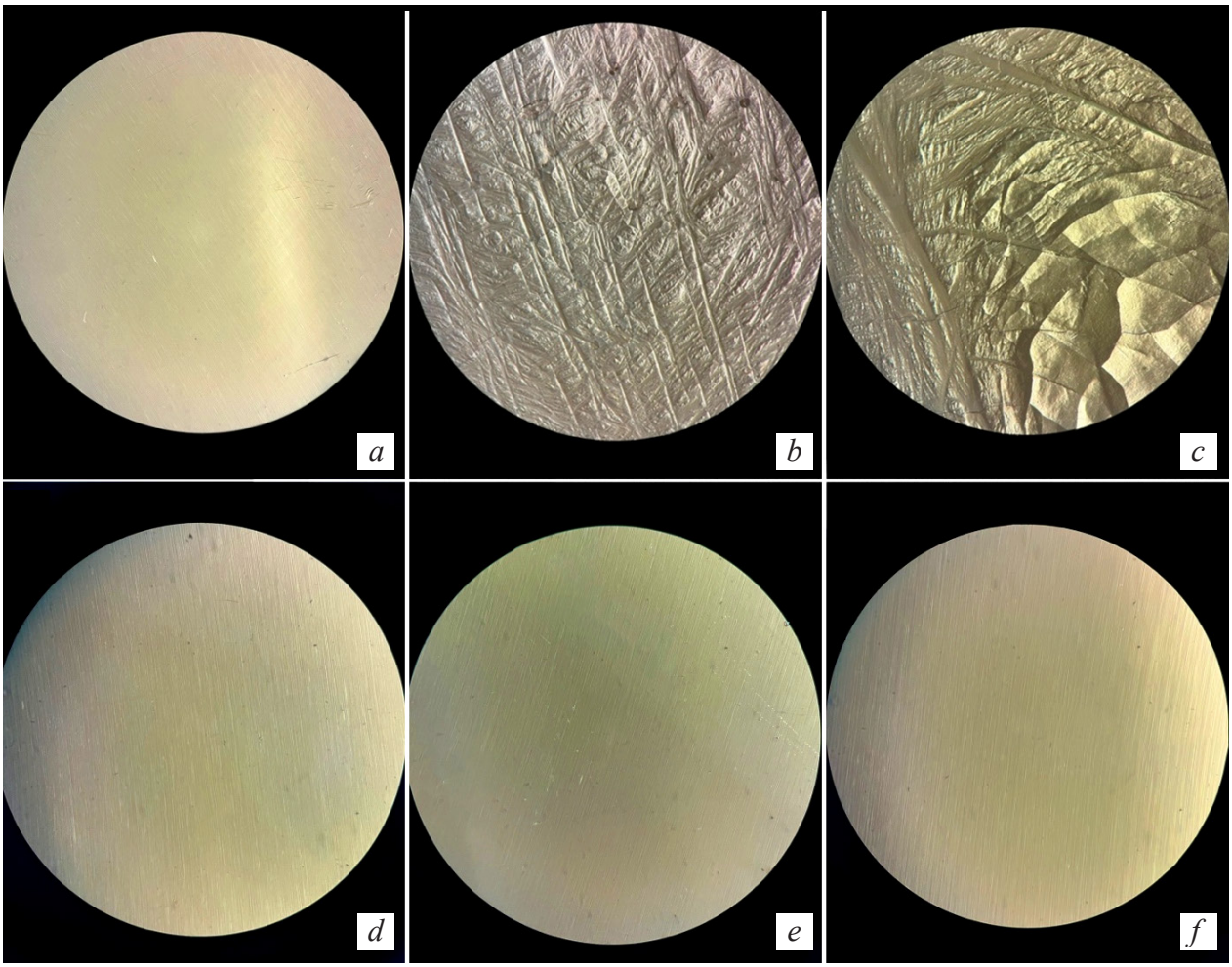

Figure 2. Surface images of (*a–c*) 3.7SmSZ and (*d–f*) 6SmSZ crystals (*a*, *d*) before and after (*b*, *e*) air and (*c*, *f*) vacuum annealing

in the *t*' phase increases, i.e., annealing of two-phase crystals drives the system to a more equilibrium state. After vacuum annealing the tetragonality degree of the crystals is lower than that after air annealing, probably indicating an additional stabilizing effect of the nonstoichiometric vacancies forming as a result of vacuum annealing.

The charge state of the samarium cations in the as-annealed crystals was checked using optical spectroscopy. Figure 4 shows luminescence spectra of the 6SmSZ crystals before and after air annealing.

The luminescence spectra before and after annealing contain bands in the green, yellow and red regions corresponding to the $^4G_{5/2} \rightarrow {}^6H_{5/2}$, $^4G_{5/2} \rightarrow {}^6H_{7/2}$ and $^4G_{5/2} \rightarrow {}^6H_{9/2}$ transitions in the Sm^{3+} ions. No bands typical of the Sm^{2+} ions were observed in the luminescence spectra. In oxide crystals such bands can be present in the 675–775 nm region. Thus one can conclude that samarium cations mainly enter the ZrO_2 lattice in the trivalent charge state and do not change their charge state after air or vacuum annealing.

Comparison of the densities of the crystals before and after annealing showed that the densities of different crystals behave in different manners as a result of annealing, depending on the content of stabilizing Sm_2O_3 (Table 2). One should however bear in mind that at comparable Sm_2O_3 concentrations the densities of the crystals

Table 1. Phase compositions, lattice parameters and tetragonality degrees of the 6SmSZ crystals before and after annealing

Specimen	Phase	Content (wt.%)	*a* (nm)	*c* (nm)	$c/\sqrt{2}a$
As-grown	*t*	60 ± 5	0.36073	0.51767	0.10147
	t′	40 ± 5	0.36438	0.51672	0.10028
Air-annealed	*t*	64 ± 5	0.36070	0.51769	0.10149
	t′	36 ± 5	0.36443	0.51670	0.10026
Vacuum-annealed	*t*	62 ± 5	0.36068	0.51764	0.10148
	t′	38 ± 5	0.36436	0.51659	0.10025

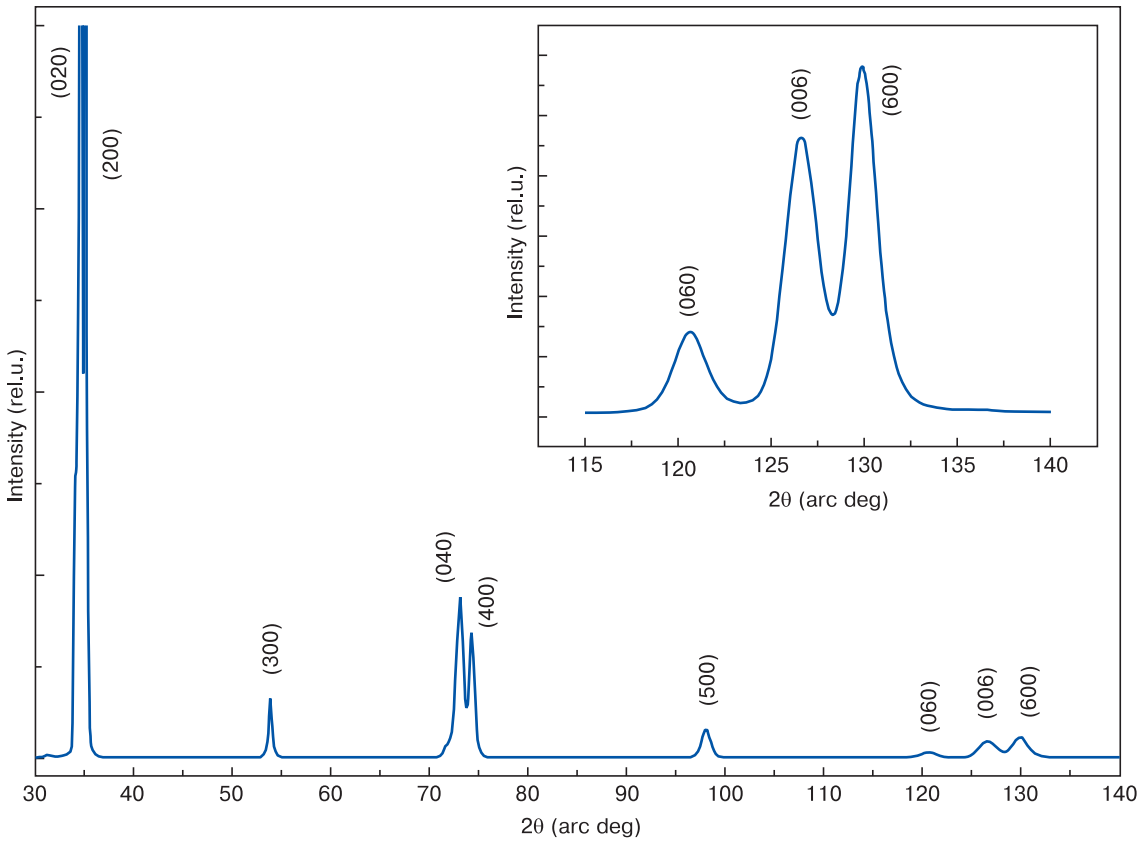

Figure 3. X-ray diffraction pattern of 3.7SmSZ specimen surface after air annealing

after vacuum annealing are always lower than those of the respective as-grown and as-air annealed crystals. This indicates the formation of high concentrations of nonstoichiometric vacancies after vacuum annealing. After air annealing the densities of the 2SmSZ, 2.8SmSZ and 6SmSZ crystals changed but slightly, whereas the densities of the other crystals decreased. This change in the crystal density can indicate a change in the phase composition of the as-annealed crystals. For example, the 2SmSZ and 2.8SmSZ crystals contained mainly the monoclinic ZrO_2 modification before and after annealing and therefore their densities after air annealing changed but a little and those after vacuum annealing decreased due to the formation of nonstoichiometric vacancies. Air and vacuum annealing of the 3.2SmSZ crystals reduced the content of the monoclinic phase in the crystal bulk and hence reduced their as-annealed densities. The noticeable decrease in the densities of the 3.7SmSZ, 4SmSZ and 5SmSZ crystals is also caused by the formation of the less dense monoclinic phase after air and vacuum heat treatment. The densities of the tetragonal 6SmSZ crystals changed but slightly after air annealing, and the but moderate reduction in their densities after vacuum annealing is possibly caused by the formation of nonstoichiometric vacancies.

Table 2. Density of as-grown and as-annealed $(ZrO_2)_{1-x}(Sm_2O_3)_x$ crystals

Specimen	Density (g/cm^3)		
	As-grown	Air-annealed	Vacuum-annealed
2SmSZ	5.890 ± 0.034	5.890 ± 0.034	5.863±0.004
2.8SmSZ	5.951 ± 0.011	5.951 ± 0.015	5.917±0.013
3.2SmSZ	6.010 ± 0.012	6.005 ± 0.012	5.997±0.008
3.7SmSZ	6.181 ± 0.008	6.012 ± 0.021	5.995±0.011
4SmSZ	6.197 ± 0.005	6.041 ± 0.021	6.031±0.008
5SmSZ	6.206 ± 0.011	6.017 ± 0.010	6.093±0.019
6SmSZ	6.264 ± 0.017	6.260±0.012	6.253±0.006

The microhardness of the as-annealed 2SmSZ, 2.8SmSZ and 6SmSZ changed but slightly as compared with the as-grown ones (Table 3). For other crystals, heat treatment reduced the microhardness, comparison between the microhardness data and the phase composition of the as-annealed crystals suggests that the decrease in the microhardness of the crystals containing 3.2 to 5 mol.% Sm_2O_3 inclusively is caused by an increase in the content or the formation of the monoclinic phase in the as-annealed crystal bulk.

Figure 5 shows diagrams illustrating the anisotropy of the crack resistance in the {100} for different indenter diagonal orientations in the specimen planes for the $(ZrO_2)_{1-x}(Sm_2O_3)_x$ crystals with $0.037 \le x \le 0.06$ before and after annealing. For the as-annealed specimens containing 2.0 и 2.8 mol.% samarium oxide, crack resistance

Table 3. Microhardness of the $(ZrO_2)_{1-x}(Sm_2O_3)_x$ crystals before and after air and vacuum annealing

Specimen	HV (GPa)		
	As-grown	Air-annealed	Vacuum-annealed
2SmSZ	8.65 ± 0.30	8.55 ± 0.30	8.50 ± 0.30
2.8SmSZ	8.75 ± 0.30	8.65 ± 0.30	8.60 ± 0.30
3.2SmSZ	10.75 ±0.30	8.75 ± 0.30	8.65 ± 0.30
3.7SmSZ	11.30 ± 0.30	9.25 ± 0.30	8.70 ± 0.30
4SmSZ	12.15 ± 0.30	9.60 ± 0.30	8.75 ± 0.30
5SmSZ	12.30 ± 0.30	10.50 ± 0.30	8.90 ± 0.30
6SmSZ	12.45 ± 0.30	12.40 ± 0.30	12.50 ± 0.30

could not be measured due to material fracture around the indentations.

Annealing of the 3.7SmSZ, 4SmSZ and 5SmSZ crystals reduced their fracture toughness by more than two-fold as compared with the as-grown figures, the fracture toughness after air and vacuum annealing being close. Unlike those crystals, annealing of the 6SmSZ solid solutions increased K_{1c} by ~ 1.5 times.

The possibility of a tetragonal-to-monoclinic transition ($t \rightarrow m$) largely affects the strength of the materials. The formation of the monoclinic phase in the crystals bulk after annealing tenders the transformation hardening mechanism in the 3.7SmSZ, 4SmSZ and 5SmSZ crystals impossible and therefore dramatically reduces their fracture toughness. The phase composition of the 6SmSZ did not change after annealing. However, 1600 °C annealing causes a redistribution of Sm_2O_3 in the t and t' tetragonal phases. The decrease in the Sm_2O_3 content in the transformable t phase after annealing can increase the efficiency of the transformation hardening mechanism and hence increase the fracture toughness of the material. One should also bear in mind the possibility of the ferroelastic hardening mechanism in the as-annealed crystals of this composition. In order to analyze the contributions of the transformation and ferroelastic hardening mechanisms to the mechanical properties of the crystals, we recorded Raman scattering spectra for the indentation areas and studied the effect of local phase composition inside and around the indentations for finding the monoclinic phase areas forming as a result of the transformation hardening mechanism. The intensity of the tetragonal-to-monoclinic phase transition (R_m) was calculated from the monoclinic and tetragonal phase band intensity ratios in the Raman spectra using the following formula [23]:

$$R_m = \frac{I^m_{178} + I^m_{190}}{I^t_{146} + I^m_{178} + I^m_{190}}. \quad (2)$$

The contribution of the ferroelastic hardening mechanism was evaluated from the orientation-dependent tetragonal phase band intensity ratios in the Raman spectra: $I(146\ cm^{-1})/I(260\ cm^{-1})$. The Raman spectra were

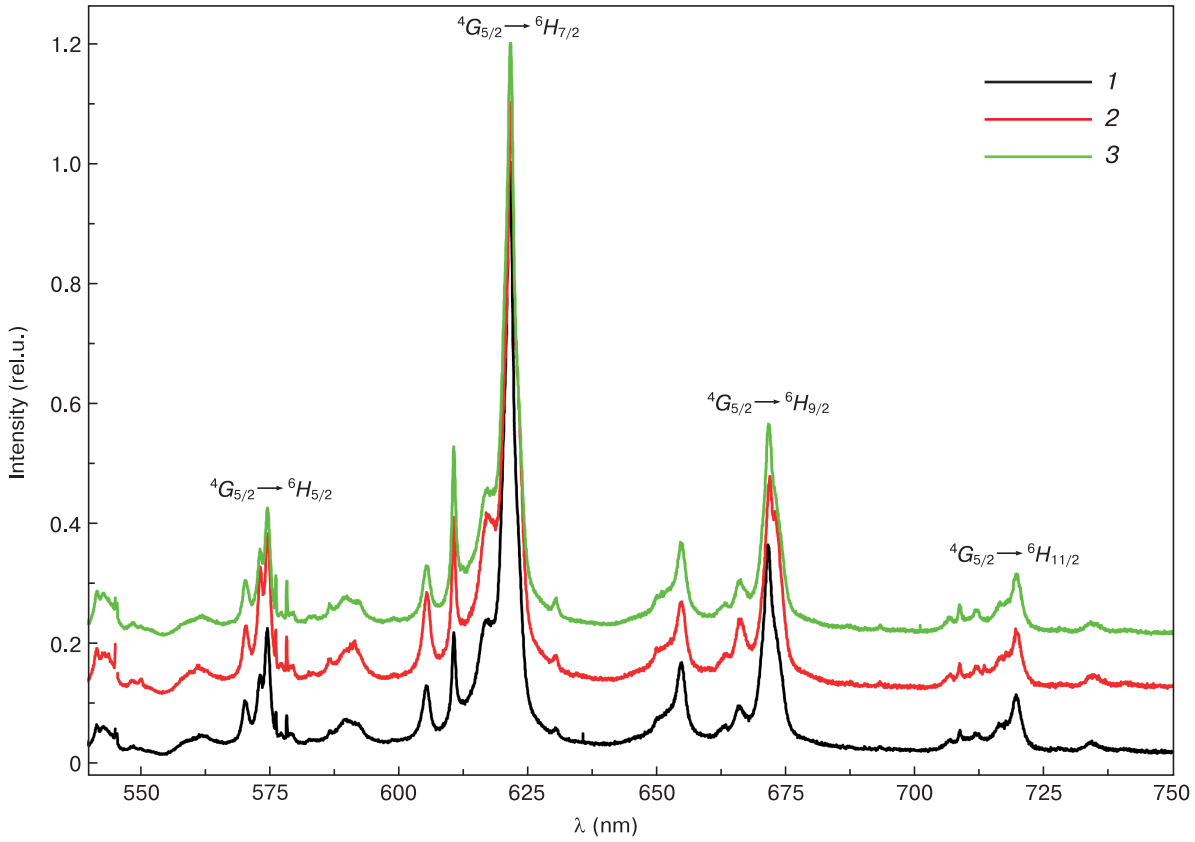

Figure 4. Luminescence spectra of 6SmSZ crystals (*1*) before and after (*2*) air and (*3*) vacuum annealing

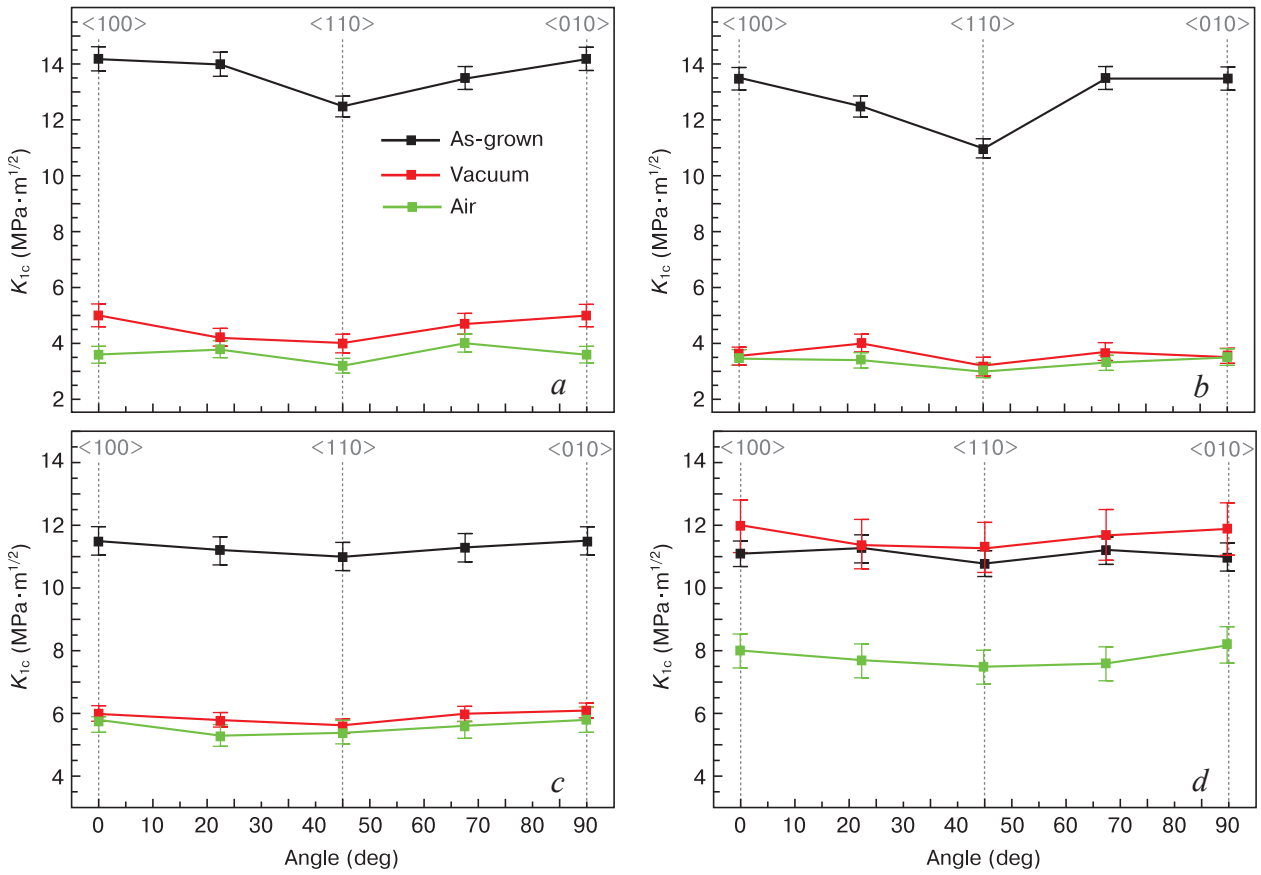

Figure 5. Anisotropy of crack resistance in {100} plane for different indenter diagonal orientation in specimen plane for (*a*) 3.7SmSZ, (*b*) 4SmSZ, (*c*) 5SmSZ and (*d*) 6SmSZ crystals before and after annealing

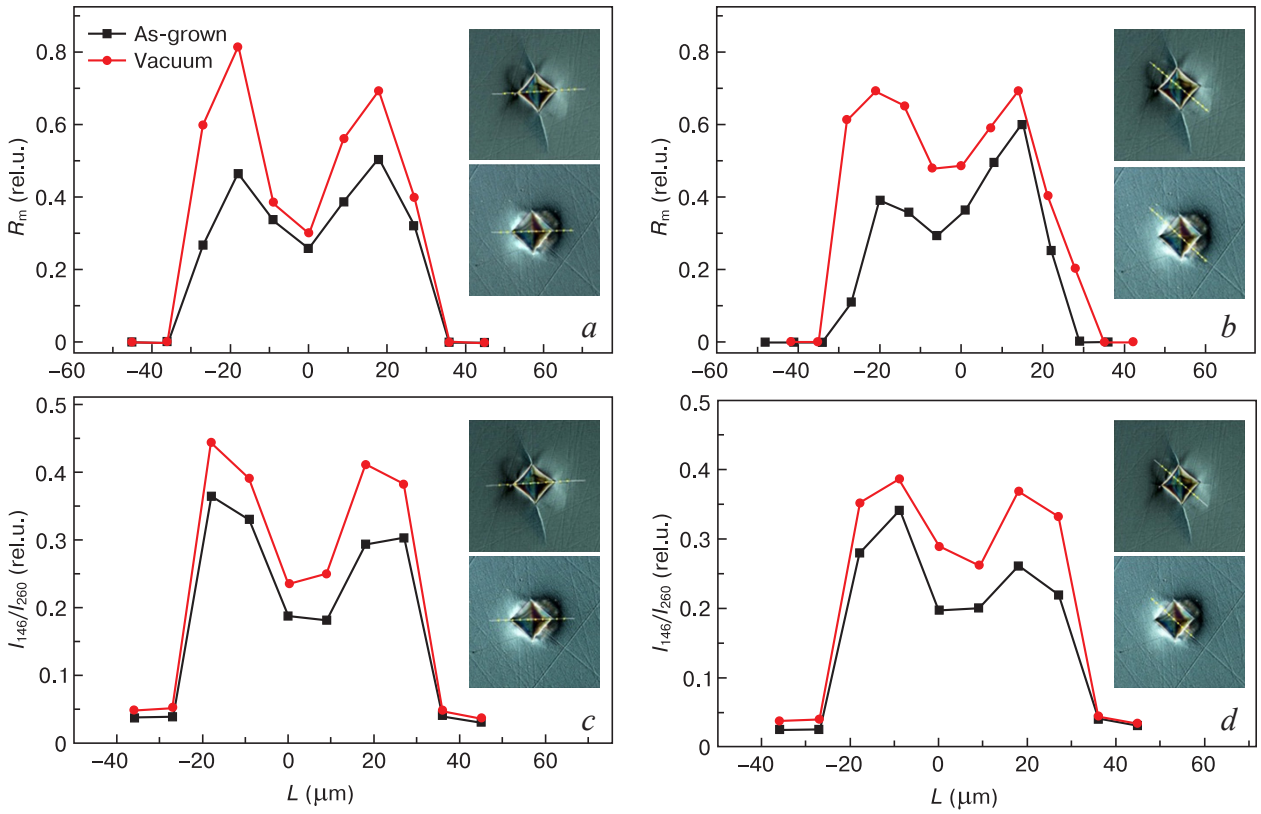

Figure 6. (*a*, *b*) tetragonal-to-monoclinic phase transition rate and (*c*, *d*) tetragonal phase band intensity ratios for 6SmSZ crystals in local areas of indentations. Inset shows indentation images with Raman spectra recording points marked

taken in local areas along indentation diagonals and laterally to indentation sides with a ~10 mm step.

Figure 6 shows monoclinic phase distributions and change in tetragonal phase band intensity ratios as one moves laterally to indentation sides for the 6SmSZ crystals before and after vacuum annealing. The patterns of monoclinic phase distribution and changes in tetragonal phase band intensity ratios in the indentation area for 6SmSZ after air annealing was similar to that for the vacuum-annealed crystals.

Figure 6 suggests that the monoclinic phase spreading region around the indentation is far greater after air annealing than for the as-grown 6SmSZ crystals. Furthermore, the formation of the monoclinic phase as a result of annealing is more rapid than in the as-grown crystals. Thus, the monoclinic phase spreading region and the rate of the tetragonal-to-monoclinic transition in the 6SmSZ crystals increases as a result of vacuum annealing, which is in agreement with the change in the tetragonality degree and accounts for the increase in the fracture toughness of these crystals as a result of heat treatment.

Evaluation of the contribution from the ferroelastic hardening mechanism from the tetragonal phase band intensity ratios in the Raman spectra showed that the orientation-dependent band intensity ratios also increase as a result of vacuum annealing.

Thus, analysis of the experimental data suggests that the fracture toughness of the as-annealed 6SmSZ crystals increases due to both the transformation and ferroelastic hardening mechanisms.

4. Conclusion

Study of the phase composition of $(ZrO_2)_{1-x}(Sm_2O_3)_x$ crystals showed that air and vacuum annealing leads to the formation monoclinic phase in all the test crystals except the 6SmSZ composition for which the lattice parameter and hence the tetragonality ratio changed as a result of annealing.

After air and vacuum annealing the Sm_2O_3 content in the *t* phase decreases and that in the *t'* phase increases, i.e., annealing of two-phase crystals drives the system to a more equilibrium state. After vacuum annealing the tetragonality degree of the crystals is lower than after air annealing, which can be accounted for by an additional stabilizing effect of nonstoichiometric vacancies forming as a result of vacuum annealing.

We showed that samarium cations mainly enter the ZrO_2 lattice in the trivalent charge state and do not change their charge state after air or vacuum annealing.

The observed changes in the microhardness and fracture toughness of the crystals are accounted for by changes in the phase composition of the crystals as a result of annealing and depend on the Sm_2O_3 concentration in the solid solutions. The formation of the monoclinic phase in the $(ZrO_2)_{1-x}(Sm_2O_3)_x$ crystals with $0.037 \le x \le 0.05$ significantly reduces the microhardness and fracture toughness of the crystals. Annealing of the $(ZrO_2)_{0.94}(Sm_2O_3)_{0.06}$ crystals increases the efficiency of the hardening mechanisms and hence increases their fracture toughness. Ferroelastic hardening provides additional contribution to the increase in the fracture toughness of the crystals. We showed that air and vacuum annealing of the $(ZrO_2)_{0.94}(Sm_2O_3)_{0.06}$ crystals increases the fracture toughness of the crystals by 1.5 times in comparison with that of the as-grown crystals.

Acknowledgements

The work was financially supported by Russian Science Foundation Grant No. 22-29-01220.

References

1. Basu R.N. Materials for solid oxide fuel cells. In: *Basu S. (Eds). Recent trends in fuel cell science and technology.* New York, NY: Springer; 2007. P. 286–331. https://doi.org/10.1007/978-0-387-68815-2_12
2. Clarke D.R., Oechsner M., Padture N.P. Thermal-barrier coatings for more efficient gas-turbine engines. *MRS Bulletin.* 2012; 37(10): 891–898. https://doi.org/10.1557/mrs.2012.232
3. Yildirim H., Pachter R. Extrinsic dopant effects on oxygen vacancy formation energies in ZrO_2 with implication for memristive device performance. *ACS Applied Electronic Materials*. 2019; 1(4): 467–477. https://doi.org/10.1021/acsaelm.8b00090
4. Hongsong Z., Jianguo L., Gang L., Zheng Z., Xinli W. Investigation about thermophysical properties of $Ln_2Ce_2O_7$ (Ln = Sm, Er and Yb) oxides for thermal barrier coatings. *Materials Research Bulletin.* 2012; 47(12): 4181–4186. https://doi.org/10.1016/j.materresbull.2012.08.074
5. Guo L., Guo H., Ma G., Gong S., Xu H. Phase stability, microstructural and thermo-physical properties of $BaLn_2Ti_3O_{10}$ (Ln = Nd and Sm) ceramics. *Ceramics International*. 2013; 39(6): 6743–6749. https://doi.org/10.1016/j.ceramint.2013.02.003
6. Wei X., Hou G., An Y., Yang P., Zhao X., Zhou H., Chen J. Effect of doping CeO_2 and Sc_2O_3 on structure, thermal properties and sintering resistance of YSZ. *Ceramics International*. 2021; 47(5): 6875–6883. https://doi.org/10.1016/j.ceramint.2020.11.032
7. Liu X.Y., Wang X.Z., Javed A., Zhu C., Liang G.Y.The effect of sintering temperature on the microstructure and phase transformation in tetragonal YSZ and LZ/YSZ composites. *Ceramics International*. 2016; 42(2): 2456–2465. https://doi.org/10.1016/j.ceramint.2015.10.046

8. Evans A.G., Mumm D.R., Hutchinson J.W., Meier G.H., Pettit F.S. Mechanisms controlling the durability of thermal barrier coatings. *Progress in Materials Science*. 2001; 46(5): 505–553. https://doi.org/10.1016/S0079-6425(00)00020-7
9. Vaßen R., Jarligo M.O., Steinke T., Mack D.E., Stöver D. Overview on advanced thermal barrier coatings. *Surface and Coatings Technology*. 2010; 205(4): 938–942. https://doi.org/10.1016/j.surfcoat.2010.08.151
10. Bahamirian M., Hadavi S.M.M., Farvizi M., Rahimipour M.R., Keyvani A. Phase stability of ZrO_2 9.5Y_2O_3 5.6Yb_2O_3 5.2Gd_2O_3 compound at 1100 °C and 1300 °C for advanced TBC applications. *Ceramics International*. 2019; 45(6): 7344–7350. https://doi.org/10.1016/j.ceramint.2019.01.018
11. Bobzin K., Zhao L., Öte M., Königstein T. A highly porous thermal barrier coating based on Gd_2O_3–Yb_2O_3 co-doped YSZ. *Surface and Coatings Technology.* 2019; 366: 349–354. https://doi.org/10.1016/j.surfcoat.2019.03.064
12. Shi Q., Yuan W., Chao X., Zhu Z. Phase stability, thermal conductivity and crystal growth behavior of RE_2O_3 (RE = La, Yb, Ce, Gd) co-doped Y_2O_3 stabilized ZrO_2 powder. *Journal of Sol-Gel Science and Technology.* 2017; 84(1): 341–348. https://doi.org/10.1007/s10971-017-4483-z
13. Chen D., Wang Q., Liu Y., Ning X. Microstructure, thermal characteristics, and thermal cycling behavior of the ternary rare earth oxides (La_2O_3, Gd_2O_3, and Yb_2O_3) co-doped YSZ coatings. *Surface and Coatings Technology.* 2020; 403: 126387. https://doi.org/10.1016/j.surfcoat.2020.126387
14. Sharma A. Witz G., Howell P.C., Hitchman N. Interplay of the phase and the chemical composition of the powder feedstock on the properties of porous 8YSZ thermal barrier coatings. *Journal of the European Ceramic Society.* 2021; 41(6): 3706–3716. https://doi.org/10.1016/j.jeurceramsoc.2020.10.062
15. Bisson J.F., Fournier D., Poulain M., Lavigne O., Mévrel R. Thermal conductivity of yttria-zirconia single crystals, determined with spatially resolved infrared thermography. *Journal of the American Ceramic Society*. 2000; 83(8): 1993–1998. https://doi.org/10.1111/j.1151-2916.2000.tb01502.x
16. Fan W., Wang Z.Z., Bai Y., Che J.W., Wang R.J., Ma F., Tao W.Z., Liang G.Y. Improved properties of scandia and yttria co-doped zirconia as a potential thermal barrier material for high temperature applications. *Journal of the European Ceramic Society*. 2018; 38(13): 4502–4511. https://doi.org/10.1016/j.jeurceramsoc.2018.06.002
17. Raghavan S., Wang H., Porter W.D., Dinwiddie R.B, Mayo M.J. The effect of grain size, porosity and yttria content on the thermal conductivity of nanocrystalline zirconia. *Scripta Materialia.* 1998; 39(8): 1119–1125.
18. Loganathan A., Gandhi A.S. Toughness evolution in Gd-and Y-stabilized zirconia thermal barrier materials upon high-temperature exposure. *Journal of Materials Science*. 2017; 52: 7199–7206. https://doi.org/10.1007/s10853-017-0956-2
19. Ponnuchamy M.B., Gandhi A.S. Phase and fracture toughness evolution during isothermal annealing of spark plasma sintered zirconia co-doped with Yb, Gd and Nd oxides. *Journal of the European Ceramic Society*. 2015; 35(6): 1879–1887. https://doi.org/10.1016/j.jeurceramsoc.2014.12.027
20. Rebollo N.R., Gandhi A.S., Levi C.G. Phase stability issues in emerging TBC systems. *High Temperature Corrosion and Materials Chemistry IV.* 2003: 431–442.
21. Borik M.A., Chislov A., Kulebyakin A., Lomonova E., Milovich F., Myzina V., Ryabochkina P., Sidorova N., Tabachkova N. Phase composition and mechanical properties of Sm_2O_3 partially stabilized zirconia crystals. *Crystals.* 2022; 12(11): 1630. https://doi.org/10.3390/cryst12111630
22. Niihara K.A fracture mechanics analysis of indentation-induced Palmqvist crack in ceramics. *Journal of Materials Science Letters.* 1983; 2: 221–223. https://doi.org/10.1007/BF00725625
23. Chien F.R., Ubic F.J., Prakash V., Heuer A.H. Stress-induced martensitic transformation and ferroelastic deformation adjacent microhardness indents in tetragonal zirconia single crystals. *Acta Materialia*. 1998; 46(6): 2151–2171. https://doi.org/10.1016/S1359-6454(97)00444-8